RSC Advances

ROYAL SOCIETY OF CHEMISTRY

www.rsc.org/advances

Journal Name

ARTICLE

Carbon-doped ZnO Submicron Spheres Functionalized with Carboxylate Groups and Effect of Dispersion Stability in the Colloidal System for High Photocatalytic Activity

Received 00th January 20xx,
Accepted 00th January 20xx

DOI: 10.1039/x0xx00000x

www.rsc.org/

JaeSoul Lee‡[a], Hyung-Seok Lim‡[a] and Kyung-Do Suh*[a]

In this work, we propose a facile fabrication method for C-doped zinc oxide (ZnO) submicron spheres using ionizable surface groups without an additional surface modification process after heat treatment. The synthetic method is comprised of diffusion of zinc precursors into pH-responsive polymer microspheres and a subsequent heat treatment step. After heat treatment at a certain temperature, the ionizable functional groups remaining on the surface of C-doped ZnO submicron spheres resulted in improved dispersion stability of the spheres in the fluid colloidal system. Using the photocatalytic activity test, the relationship between dispersion stability and the photocatalytic property of the C-doped ZnO submicron spheres was investigated. As a result, the content of carbon atoms and the surface functional groups depended on the pH of the reaction medium.

Introduction

With continuous economic growth and rapid industrial development in international society, pollution by organic matter is considered one of the most serious environmental problems. In order to solve this problem, many countries have tried to develop eco-friendly and sustainable energy technologies (photocatalysts, secondary batteries, solar cells). As a method for processing environmental pollution, semiconductor photocatalysis technology is able to effectively degrade and remove organic compounds and chemical toxins (toxic gas or pollutants) from the surroundings.[1, 2] As a result, many semiconductor materials have been studied for environmental remediation. Metal oxides (ZnO, TiO_2, SiO_2, Fe_2O_3, CuO) in photocatalysts have especially good potential as photo-sensitive semiconductors.[3-7] Among them, zinc oxide (ZnO) has a wide band gap (3.2 eV)[8], large excitonic binding energy (60 meV) that results in more efficient excitonic emission at room temperature[9], and fascinating features including physical and chemical stability, high catalytic activity, low cost, environmental sustainability, and high photosensitivity.[10-12] However, its photocatalytic activity is unstable due to its wide band gap energy, rapid recombination rate of photogenerated electron-hole pairs, and low photoenergy-conversion efficiency.[13] To improve the photocatalytic performance of ZnO, band gap energy has been adjusted in various ways such as doping with a non-metal or transition metal or creating a composite with other small-band gap semiconductors. Among them, the techniques for doping with non-metal species (C, N or S) have attracted attention as a way to overcome the drawbacks of ZnO.[14] A carbon dopant has been widely used to modify thermal stability, bandgap narrowing, adsorbability, and electronic properties of semiconductors.[15, 16] To date, many researchers have reported that carbon dopant in ZnO photocatalysts can extend the light absorption range and hinder the recombination of photogenerated electrons and holes at suitable doping levels because of the narrow bandgap and good electron conductivity.[17] For convenience and recycling of photocatalysts, C-doped ZnO photocatalysts are typically synthesized as a thin film consisting of nanomaterials that are prepared using various synthetic methods such as precipitation[18], hydrothermal[19], template-based growth[20] and solvothermal[21]. However, these methods have some disadvantages such as high cost, a complex process, stringent reaction conditions, and difficult control of the doped carbon content in semiconductors. Control of the amount of doped carbon is very important because, if the carbon content on the surface of ZnO is too high, it can inhibit the light activity.[22-24] The fluid colloidal system is more suited than a thin film to maximize the efficiency of photocatalysts because the separated semiconductor particles offer more active sites for adsorption of organic pollutants, increasing the occurrence of interfacial reactions. Nevertheless, the colloidal system using

[a] Department of Chemical Engineering, College of Engineering, Hanyang University, Seoul, Republic of Korea, 133-791. E-mail: kdsuh@hanyang.ac.kr
* Corresponding author (kdsuh@hanyang.ac.kr)
‡ These authors contributed equally to this work.

Electronic Supplementary Information (ESI) available: [SEM images, TGA curve and FT-IR spectrum of poly(MAA/EGDMA) microspheres; SEM images of pure ZnO nanoparticles; HR-TEM image and FT-IR spectra of C/ZnO submicron spheres prepared in aqueous solutions with different pHs; The photocatalytic degradation (under 300W UV irradiation) of MB over C/ZnO submicron spheres prepared in aqueous solution with pH 7.6; Nitrogen adsorption-desorption isotherms and pore size distribution plots of C-doped ZnO fabricated in aqueous solutions with different pHs; SEM images, XRD patterns and FT-IR spectra of C/ZnO submicron spheres prepared with different temperatures]. See DOI: 10.1039/x0xx00000x

photocatalyst particles has not been widely studied. In a fluid colloidal system, the dispersion stability of the semiconductor particles enhances the photocatalytic efficiency for a long time. Since the photocatalytic degradation reaction occurs through reaction of photogenerated electrons and holes on the surfaces of the semiconductor particles, if the dispersion stability of the semiconductor particles is unstable, the photocatalytic efficiency will be reduced due to creaming, sedimentation, flocculation, or coalescence of the particles. There are some studies on the enhanced dispersion stability of nano-sized photocatalysts through surface modification processes such as those of chemical surfactants.[25] However, some toxic surfactants must be removed for a practical application.

In this paper, we suggest a facile fabrication method of C-doped ZnO submicron spheres with good dispersion stability using poly(methacrylic acid/ethylene glycol dimethacrylate) [poly(MAA/EGDMA)] microspheres as a template without an additional surface modification process. Since pH-responsive polymer templates have a tunable storage capacity for Zn metal precursors, the amount of carbon atoms doped in the resulting ZnO submicron spheres is easily controlled by adjusting the pH of the reaction medium. Additionally, the ionizable functional groups of the carbon residue remaining on the surfaces of the ZnO submicron spheres can improve the dispersion stability. As a result, the photocatalytic performance of ZnO submicron spheres is closely connected to carbon doping and dispersion stability in the aqueous solution. The effects on the amount of carbon doped in ZnO submicron spheres and the remaining functional groups on the particle surfaces are discussed in this study.

Results and discussion

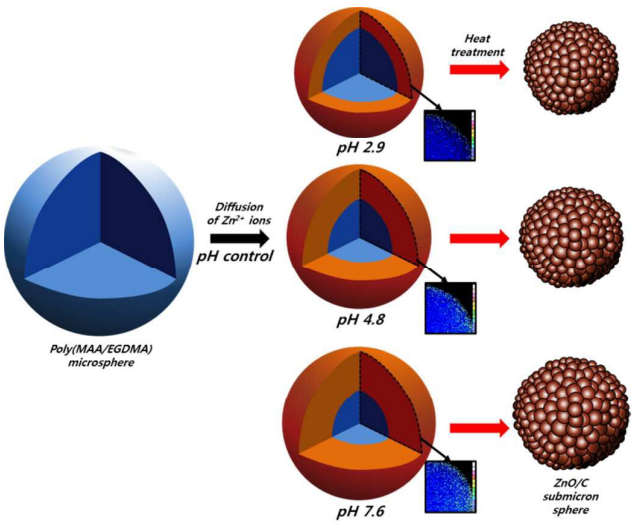

Scheme 1. Schematic illustration of the fabrication process of the C-doped ZnO submicron spheres using reaction media with three different pHs.

In this work, pH-responsive poly(MAA/EGDMA) microspheres were used as a sacrificial template for C-doped ZnO submicron spheres. Zn precursors from zinc acetate dihydrate can exist as Zn^{2+} and $Zn(OH)_2$ in an aqueous solution. Since the fabrication strategy in this study is based on the electrostatic attraction between the Zn precursors and ionized carboxyl groups of the polymer backbone, the amount of Zn precursors diffusing into the templates depends on the pH of the reaction system. Three types of samples were prepared by adjusting the pH (2.9, 4.8, and 7.6) of the reaction media and applying heat treatment, as illustrated in Scheme 1.

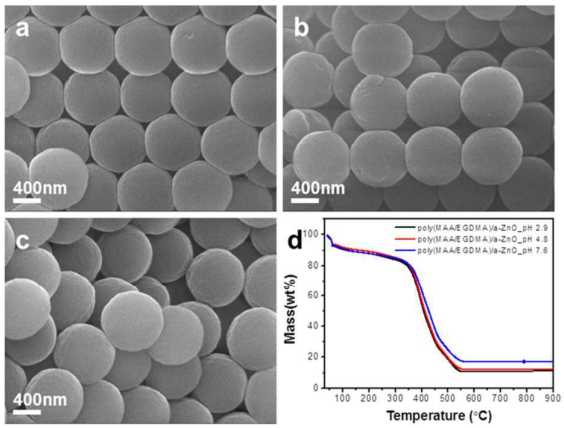

Figure 1. SEM images of poly(MAA/EGDMA)/amorphous ZnO microspheres synthesized in aqueous solutions with three different pHs; (a) 2.9, (b) 4.8, and (c) 7.6. TGA curves of the three samples.

Figures 1a, b, and c show SEM images of the poly(MAA/EGDMA)/amorphous ZnO microspheres prepared in solutions with different pHs (2.9, 4.8, and 7.6). The morphologies of the three samples were similar to that of poly(MAA/EGDMA) microspheres before introduction of the zinc precursors (Figure S1). However, after the introduction of the zinc precursors, the particle size increased as the pH of the medium increased. Figure 1d shows that the TGA curves of the three samples have similar thermal degradation processes, while different residual masses were exhibited. With the increase in temperature, the polymer phase in the composite microspheres decomposed rapidly from 380 °C. For the samples prepared at pH 2.9 and 4.8, the residue accounted for approximately 20% of the composition at 500 °C, while the sample prepared at pH 7.6 left approximately 25% residue. At pH 7.6, the polymer phase absorbed more of the water in contact with the Zn precursors via polar groups in the polymer backbone than at pH 2.9 and 4.8. HR-TEM and EDX mapping images were analyzed to investigate the morphologies of Zn precursors introduced into the polymer phase at different pHs. Despite the large amount of Zn precursor, as illustrated in Figure 1d, the three samples exhibited a smooth surface, and there was no difference in the HR-TEM images of the three samples prepared at different pHs, as shown in Figures 2a, b, and c. Alternatively, the EDX spectroscopy elemental maps interestingly demonstrated that the concentration and location of Zn atoms introduced to the polymer phase were

quite different in the three samples. The concentration of Zn atoms in the composite microspheres prepared in the aqueous pH 7.6 solution was greater than that of the two samples prepared at pH 2.9 and 4.8. Accordingly, the carbon concentration decreased as the number of Zn atoms increased, as shown in Figures 2d, e, and f. For the sample prepared at pH 7.6, the Zn atoms were well dispersed throughout the polymer phase. These results indicate that the Zn precursors were introduced from the surface to the center of the polymer microsphere, and the amount of introduced Zn precursor can be controlled by adjusting the pH of the reaction medium.

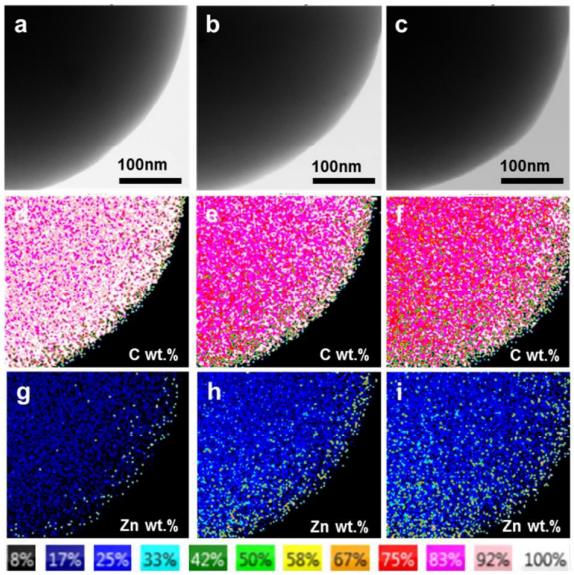

Figure 2. HR-TEM and EDX mapping images of the poly(MAA/EGMDA)/amorphous ZnO microspheres prepared in aqueous solutions with different pHs; 2.9 (a, d and g), 4.8 (b, e and h), and 7.6 (c, f and i).

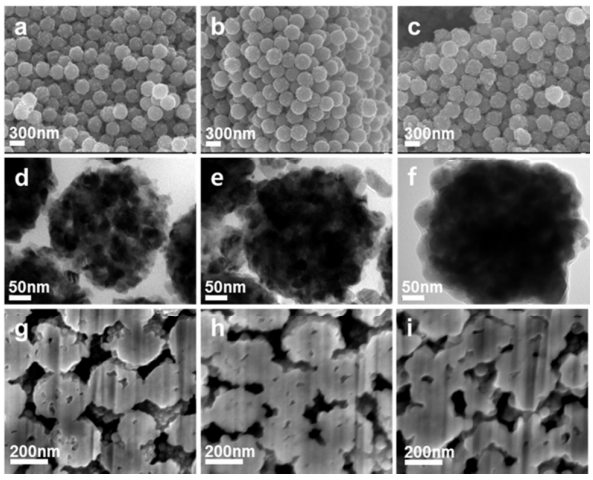

Figure 3. SEM, TEM, and FIB-SEM images of C-doped ZnO submicron spheres prepared in aqueous solutions with different pHs after subsequent heat treatment at 500 °C for 2h in air flow; pH 2.9 (a, d and g), pH 4.8 (b, e and h), and pH 7.6 (c, f and i).

Figure 3 shows the SEM, TEM, and FIB-SEM images of C-doped ZnO submicron spheres obtained after poly(MAA/EGDMA)/amorphous ZnO microspheres were synthesized under one of three different pH conditions and subsequent heat treatment at 500 °C. SEM images illustrate uneven particle surfaces of the three heated samples and different average particle diameters. The average diameters of the C-doped ZnO submicron spheres in the three pH solutions were 310, 325, and 362 nm, respectively (To obtain the number average particle size, around 100 particles in one SEM image were analysed with Adobe Photoshop software). The particle size of the C-doped ZnO submicron spheres increased as the pH increased because the amount of Zn precursors introduced into the polymer phase increased at higher pH, as shown in Figure 3. TEM images of the three samples show that a submicron sphere consisted of several nano-grains; consequently, all samples had a porous structure, as shown in Figures 3d, e, and f. The cross-sectional images observed with FIB-SEM clearly illustrate that the C-doped ZnO submicron spheres had internal pores. After the Zn precursors were introduced into the three-dimensional colloidal networks, the heat-treated sample was composed of nano-sized ZnO particles rather than single, submicron particles as the

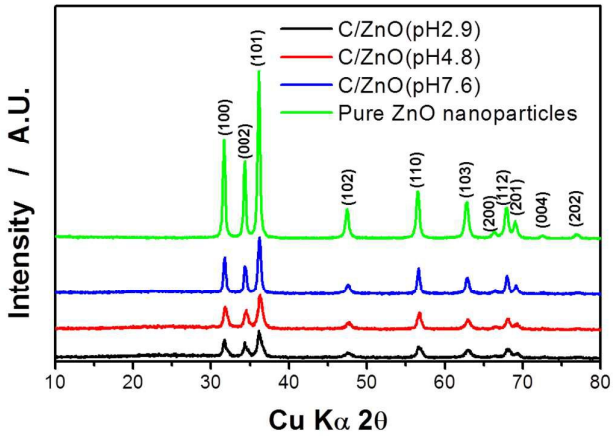

remaining residue from the polymer phase acted as a barrier to prevent the growth for a large size particle.[26]

Figure 4. X-ray diffraction patterns of C-doped ZnO submicron spheres prepared in aqueous solutions with different pHs after subsequent heat treatment at 500 °C for 2h in air flow; pH 2.9 (black), pH 4.8 (red), pH 7.6 (blue), and pure ZnO nanoparticles (green).

Figure 4 shows XRD patterns of three C-doped ZnO samples prepared under different pH conditions and pure ZnO nanoparticles synthesized via the same experimental conditions without the polymer template. All samples exhibited several peaks corresponding to the (100), (002), (101), (102), (110), (103), (200), (112), (201), (004) and (202) planes, which are typical of hexagonal wurtzite ZnO (JCPDS-80-0074). The HR-TEM image of C-doped ZnO submicron spheres fabricated at pH 7.6 shows a d-spacing of 0.26 nm, corresponding to the interspacing of the (002) lattice plane, as shown in Figure S3. Additionally, the three C-doped ZnO

samples displayed a red-shift of the diffraction peaks to the 2θ angle, which is ascribed to residual stress and the doped carbon effect in the crystalline ZnO.[22, 27] These results suggest that our synthetic system using pH-responsive polymer microspheres is an effective way to prepare carbon-doped metal oxide particles. Compared to pure ZnO, C-doped ZnO displays low intensity peaks because carbon residues remaining in the heated samples hinder the crystal growth of ZnO, resulting in a reduction in the intensity of diffraction peaks.

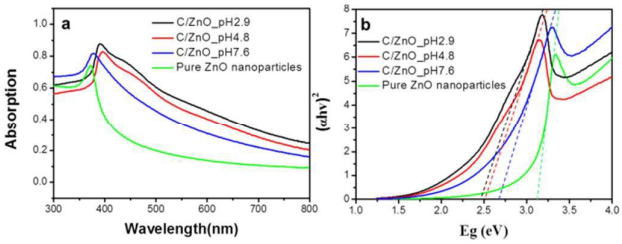

Figure 5. (a) UV-visible diffuse reflectance spectra, and (b) Tauc plots for estimating the band gap energies of pure ZnO and C-doped ZnO submicron spheres prepared in aqueous solutions with different pHs and subsequent heat treatment at 500 °C for 2h in air flow; pH 2.9 (black), pH 4.8 (red), pH 7.6 (blue), and pure ZnO nanoparticles (green).

To compare the optical properties of all samples, the UV-visible diffuse reflectance spectra and Tauc plots were analyzed, as shown in Figure 5. The absorption characteristics of pure ZnO and C-doped ZnO submicron spheres were different. The C-doped ZnO submicron spheres fabricated using polymer microspheres demonstrated enhanced light absorption and a significant red shift of the optical bandgap edge into the visible-light region. Consequently, the C-doped ZnO submicron spheres had low band gap energy. These results are attributed to the carbon atoms in the ZnO submicron spheres after heat treatment.[28]

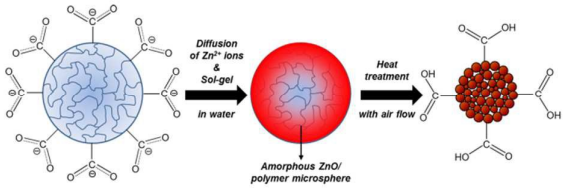

Scheme 2. Schematic illustration of the facile fabrication method of C-doped ZnO submicron spheres with ionizable functional groups using pH-responsive polymer microspheres.

ZnO microspheres contained carbon atoms throughout the submicron particle. In addition, a small amount of the carboxylic acid groups of the polymer backbone remained on the surfaces of the C-doped ZnO submicron spheres after heat treatment at 500°C, as illustrated in Scheme 2. There are two primary reasons for this result. First, after Zn precursors were introduced into the polymer microspheres, $(–COO^-)_2\ Zn^{2+}$ was formed in the polymer phase and improved the thermal stability of the composite microspheres during heat treatment. In general, the introduction of metal ions into the polymer phase with carboxylic acid (–COOH) groups can modify the physicochemical properties of the polymer films such as electrical properties, water adsorption, viscosity, and thermal stability.[29] In these experiments, most of the poly(MAA/EGDMA) microspheres prepared using the distillation-precipitation method were decomposed at temperatures less than 500°C, as shown in Figure S1c. However, the thermal characteristics of the polymer microspheres were changed by introduction of Zn precursors. Since the –COOH groups can be in the form of a carboxylate ($–COO^-$) through proton exchange under the neutral condition, Zn^{2+} in an aqueous solution has strong interaction with $–COO^-$ groups of the polymer back bone. The thermal stability of poly(MAA/EGDMA)/Zn precursor composite microspheres improved as the $(–COO^-)_2\ Zn^{2+}$ form increased in the polymer phase, as shown in Figure 1d. Thus, the functional groups remained after growth of ZnO nano-crystals at 500°C due to better thermal stability of the $(–COO^-)_2\ Zn^{2+}$ form than the –COOH groups. Secondly, it is also important that the Zn precursors are diffused into the polymer phase and not adsorbed onto the surfaces of the polymer microspheres, as shown in the HR-TEM and EDX mapping images (Figure 2). Therefore, two-step purification via repetitive centrifugation with ethanol and water was used to remove the Zn precursors adsorbed on the surfaces of the polymer microspheres.

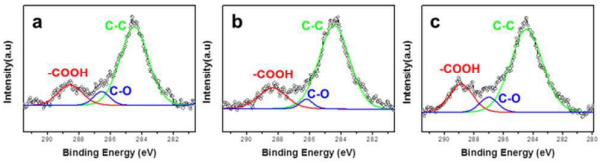

Figure 6. C1s XPS spectra of C-doped ZnO submicron spheres prepared in aqueous solutions with different pHs and subsequent heat treatment at 500 °C for 2h in air flow; (a) pH 2.9, (b) pH 4.8, and (c) pH 7.6.

XPS was conducted to analyze the surface characteristics of all C-doped ZnO submicron spheres. The XPS peaks corresponding to C 1s are shown in Figure 6. Peaks of C 1s belong to the carbon-oxygen compounds, such as sp3, C-OH and COOH, which remained on the surfaces of the C-doped ZnO submicron spheres. The FT-IR spectra show that the carboxylic acid groups were ionized on the surfaces of C-doped ZnO submicron spheres fabricated at pH 7.6, as shown in Figure S4. In addition, the atomic percentages of the surface carbons of the three samples fabricated in aqueous solutions with different pHs were 9.88% (pH 2.8), 11.72% (pH 4.8), and 12.53% (pH 7.6), respectively. This result shows that the amount of Zn precursors introduced into the outer phase of the polymer microspheres had an effect on the remaining surface groups of the grown ZnO submicron spheres after heat treatment. Since the carboxylic acid groups were ionized and had a negative charge, the physical properties of samples in the aqueous solution were investigated. The average particle size and zeta potential values of all samples dispersed in the aqueous solutions are listed in Table 1. Despite the fact that

pure ZnO nanoparticles have a nano-size diameter in the dried condition, as shown in the SEM images (Figure S3), the average particle size was approximately 2800 nm in an aqueous solution. The average diameter of the C-doped ZnO submicron spheres fabricated under acidic conditions in a colloidal system was 2125 nm, while they had an average submicron size of 310 nm in the atmosphere. Alternatively, the particle diameters of two samples fabricated in aqueous solutions with pH 4.8 and 7.6 were 299.7 and 318.2 nm, respectively. This phenomenon can be explained by the zeta potential measurement.

Sample	Particle size in aqueous solution after ultra-sonication (nm)	Zeta potential (mV)
Pure ZnO	2803	-3.47
C/ZnO-pH 2.9	2125	-10.3
C/ZnO-pH 4.8	299.7	-27.8
C/ZnO-pH 7.6	318.2	-38.0

Table 1. Average particle size and zeta potential values of pure ZnO nanoparticles and C-doped ZnO submicron spheres fabricated in aqueous solutions with different pHs.

The zeta potential values of the three samples fabricated using a polymer template increased as the pH level of the reaction medium increased. In general, it is possible that colloids are in a stable when the zeta potential exceeds ±30 mV. The zeta potential values in Table 1 demonstrate why the average particle diameters of the dried samples were quite different than those in an aqueous solution. Therefore, the dispersion state of the colloids was closely related to the remaining functional groups on the surfaces of the C-doped ZnO submicron spheres fabricated using pH-responsive polymer microspheres.

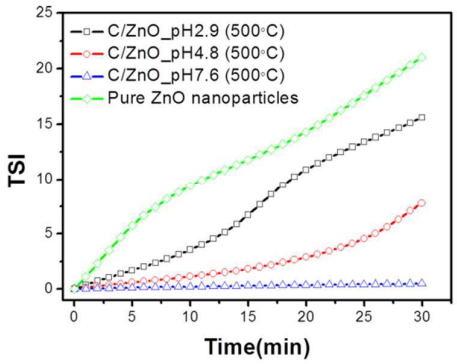

Figure 7. Dispersion stability of the pure ZnO nanoparticles and C-doped ZnO submicron spheres fabricated in aqueous solutions with different pHs and further heat treatment at 500 °C for 2h in air flow; pH 2.9 (black), pH 4.8 (red), pH 7.6 (blue), and pure ZnO nanoparticles (green).

Figure 7 shows the dispersion stability of all samples in a colloidal system. After all colloidal solutions were prepared by mechanical stirring with ultra-sonication, the dispersion stability was measured for 30 min using a Turbiscan dispersion stability analyzer without agitation. The Turbiscan stability index (TSI) represents the change in dispersion stability with time, and a larger TSI value indicates poor dispersion stability. Compared to pure ZnO, the three kinds of C-doped ZnO submicron spheres showed better dispersion stability. The sample fabricated at pH 7.6 especially exhibited very good dispersion stability for 30 min. The dispersion characteristics of all colloidal solutions were well matched with the zeta potential values, as shown in Table 1. In other words, it is important that the charge repulsive force of the photocatalyst particles is stable in an aqueous solution.

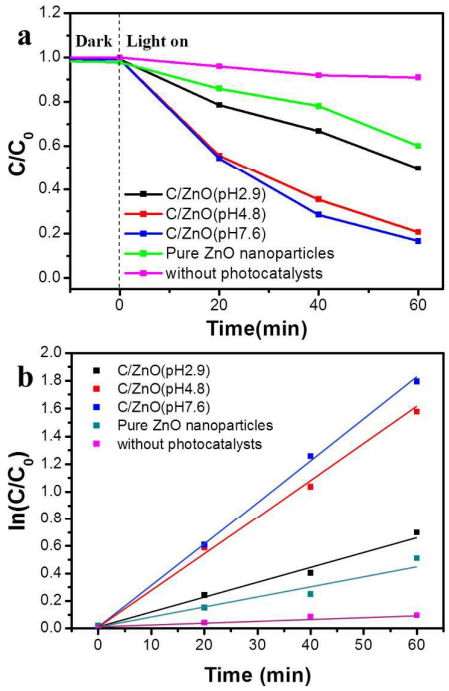

Figure 8. The photocatalytic degradation (under 16 W UV irradiation) of MB over pure ZnO nanoparticles and C-doped ZnO submicron spheres prepared in aqueous solutions with different pHs and subsequent heat treatment at 500 °C for 2h in air flow; pH 2.9 (black), pH 4.8 (red), pH 7.6 (blue), and pure ZnO nanoparticles (green): (a) change in the MB concentration as a function of time; (b) estimation of the initial reaction rate constant.

Figure 8 show the photocatalytic degradation of MB against the C-doped ZnO submicron spheres and pure ZnO nanoparticles under UV irradiation from a 16 W lamp. The power of the light is an essential factor for photocatalytic performance because the degradation of MB molecules strongly depends on the light intensity. Figure S5 shows the photocatalytic degradation of MB using C-doped ZnO submicron spheres fabricated at pH 7.6 under UV irradiation from a 300 W UV lamp. A very fast degradation rate was exhibited under the 300 W UV lamp. However, this performance was not attributed to the pure photocatalytic

activity of the C-doped ZnO sample. In our previous work, we reported that MB molecules in an aqueous solution were decomposed by the high temperature from a strong UV light.[30] Thus, a weak UV light (16 W) was used to measure the precise photodegradation performance of the photocatalysts. All photocatalyst powders were prepared in the dark with magnetic stirring for 1 h before UV light irradiation. In this step, all samples showed poor adsorption of MB, which might be due to the very low surface areas of the samples, as shown in Figure S6. However, the photocatalytic efficiencies of all samples were quite different from one another. The changes in MB concentration were analyzed as a function of UV irradiation time, as shown in figure 8a. During UV irradiation, the photocatalytic performance of the C-doped ZnO submicron spheres fabricated using polymer microspheres was better than that of pure ZnO nanoparticles. Although they have a low specific surface area, the C-doped ZnO submicron spheres fabricated at pH 4.8 and 7.6 exhibited good photocatalytic efficiencies of approximately 80% and 83%, respectively, after UV irradiation for 1 h. As expected, the sample fabricated at pH 7.6 showed the fastest rate constant of all the samples investigated, as shown in figure 8b. Good photocatalytic efficiency of C-doped ZnO submicron spheres was attributed to the dispersion stability of photocatalyst particles and the carbon doping that hinders the recombination rate of photo-generated electrons and holes at suitable doping levels. To demonstrate the effect of dispersion stability on the surface functional groups, the morphologies, chemical characteristics, and photocatalytic activities of C-doped ZnO submicron spheres were compared with and without surface functional groups. Figure S7 shows the effect of heating temperature on the morphology and crystallinity of C-doped ZnO submicron spheres. In general synthetic methods for metal oxide photocatalysts, the crystallinity of metal oxides increases as the heating temperature increases. Metal oxide photocatalysts with high crystallinity exhibit good photocatalytic activity for degradation of organic pollutants. However, in our case, despite the fact that heat-treated samples at higher temperatures of 650 and 800°C have better crystallinity, they showed poor photocatalytic activities, as shown in Figures S7, S8 and S9. Figure S8 displays the FT-IR spectra of all samples at different heating temperatures. The surface functional groups corresponding to the carboxylic acid and carboxylate groups disappeared as the heating temperature increased, whereas the peak intensity corresponding to ZnO increased. Based on these results, the most important factor to improve photocatalytic efficiency is the dispersion stability of photocatalysts in the fluid colloidal system. In order to verify the practical application, C-ZnO submicron spheres were recycled in three successive photocatalytic test, as shown in figure S10. The photocatalytic activity of C-ZnO submicron spheres prepared in pH 7.6 exhibits high photocatalytic efficiency in every cycle. Figure S11 shows SEM, TEM images, XPS and FT-IR spectra of C-ZnO submicron spheres after three-cycle test. The three C-ZnO samples after each cycle of photocatalytic degradation exhibit no significant morphological and structural changes compared to C-ZnO sample before any photocatalytic tests. Besides, the surface functional groups of the C-ZnO submicron spheres survived even after three–cycle test with photocatalytic reaction. These results show that the photocatalytic system containing colloidal C-ZnO with a good dispersion stability has reusability as well as high photocatalytic activity.

Experimental

Materials

Zinc acetate dihydrate ($(CH_3COO)_2{\cdot}2H_2O$, Aldrich), methacrylic acid (MAA, Junsei), ethylene glycol dimethacrylate (EGDMA, TCI), acetonitrile (AN, Daejung), α,α'-azobis-(isobutyronitrile) (AIBN, Junsei), methylene blue (MB, Junsei), anhydrous ethyl alcohol (EtOH, Daejung), hydrochloric acid (HCl, Samchun), sodium hydroxide (NaOH, Aldrich), and distilled water (DI water) were used as received.

Preparation of poly(MAA/EGDMA) microspheres

Poly(MAA/EGDMA) microspheres were synthesized through distillation-precipitation polymerization. All materials were reacted in a glass reactor without mechanical stirring. MAA (32g) and EGDMA (8g) were polymerized at 88 °C for 40 min in a medium consisting of AN (272g), DI water (48g), and AIBN (0.8g). EGDMA was used as a cross-linker, and AIBN was used as an initiator. After polymerization, the remaining residues were removed and purified by centrifugation with ethanol and distilled water. The precipitates were then dried in a vacuum.

Preparation of C-doped ZnO submicron spheres

Poly(MAA/EGDMA) microspheres (2 g) and pH solutions (pH 2.9, 4.8 and 7.6, 1000g) were placed in a four-neck flask and dispersed in an ultra-sonicator for 10 minutes. The solution was stirred for 2 h at 200 rpm to evenly disperse the particles. Then, zinc acetate dihydrate (2g) was dissolved in DI water (500g), poured into a flask, and continuously stirred for 3 h. After the products were centrifuged several times with ethanol and DI water at 3600 rpm to filter the residue, the products were dried in a vacuum. The as-prepared poly(MAA/EGDMA)/amorphous ZnO was heated to 500 °C at 5 °C/min and maintained for 2 h at 500 °C under air to obtain C-doped ZnO submicron spheres and allow the formation of carboxyl groups on the surface.

Characterization

All products were characterized with X-ray diffraction (XRD, D/MAX RINT 2000, Rigaku), scanning electron microscopy (SEM, JSM-6300, JEOL), focused-ion beam scanning electron microscopy (FIB-SEM, Hitachi S-4800, HITACHI), transmission electron microscopy (TEM, JEM-2000EX, JEOL), Fourier transform infrared spectroscopy (FT-IR, Nicolet 6700, Thermo scientific), high-resolution transmission electron microscopy (HR-TEM, JEM-2100F, JEOL), HR-TEM-based X-ray spectroscopy (EDX) elemental mapping analysis, Zetasizer (Nano ZS, Malvern Instruments), thermogravimetric analysis (TGA, Q500, TA Instruments), Brunauer–Emmett–Teller (BET, AS1-A4, Quantachrome), X-ray photoelectron microscopy (XPS, Theta

Probe, Thermo Fisher Scientific Co.), dispersion stability analyzer (TURBISCAN, TURBISCAN LAB, Formulation) and UV-vis spectroscopy (Carry 60, Agilent Technologies).

Photocatalytic activity tests of C-doped ZnO submicron spheres

The photocatalytic activities of C-doped ZnO submicron spheres were measured at room temperature from the degradation of MB under UV light from 16 W and 300 W lamps. Before the photocatalytic test was initiated, DI water (14g) and C-doped ZnO submicron spheres (0.02 g) were placed into an ultrasonic bath for 12 h to disperse the particles. The MB solution was composed of MB (0.006 g) and DI water (900 g). Lastly, DI water (14 g) and C-doped ZnO submicron spheres (0.02 g) were placed into the MB solution (36 g) in a quartz beaker. At this step, the concentration of the MB solution was 0.000015 M. Prior to illumination, the suspensions were stirred in the dark for 60 min to reach the adsorption-desorption equilibrium of dye molecules on the surfaces of the photocatalysts. During the degradation, 5 mL of the suspension was collected every 20 min. The used sample was then replaced with fresh sample in order to reduce error. The concentration of the MB solution was measured using an UV-vis spectrophotometer at maximum absorption wavelengths that varied with irradiation time. Recycling test was carried out three times for an hour by using C-ZnO submicron spheres prepared in pH 7.6.

Conclusions

In summary, C-doped ZnO submicron spheres were successfully synthesized using pH-responsive poly(MAA/EGDMA) microspheres. The content of the introduced zinc precursors was adjusted using pH control of the reaction medium and was measured with HR-TEM-based EDX mapping analysis and TGA data. After heat treatment at a constant temperature, the carbon atoms were doped into crystalline ZnO, and the ionizable functional groups remained on the particle surfaces. The C-doped ZnO submicron spheres exhibited a good photocatalytic efficiency of approximately 80% under UV irradiation for 1 h. This fast photodegradation rate of MB is attributed to the good dispersion stability of the C-doped ZnO submicron spheres and carbon doping that can efficiently suppress the recombination of photo-generated electrons and holes. Since this fabrication method provides a facile route to synthesize C-doped metal oxides with good dispersion stability, it will be widely applicable in various fields such as water splitting, hydrogen production, and photocatalysts.

Acknowledgements

This research was supported by Basic Science Research Program through the National Research of Korea (NRF) funded by the Ministry of Education (No. 2014R1A1A2058754).

References

1 Z. Wu, Huan Wang, Y. Xue, B. Li and B. Geng, *J. Mater. Chem. A*, 2014, **2**, 17502-17510
2 C. Han, M. Yang, B. Wengab and Y. Xu, *Phys. Chem. Chem. Phys.,* 2014, **16**, 16891-16903
3 S. Martha, K. Hemalata Reddy and K. M. Parida*, J. Mater. Chem. A*, 2014, **2**, 3621-3631
4 J. Huo, Y. Hu, H. Jiang and C. Li, *Nanoscale*, 2014, **6**, 9078-9084
5 D. Zhang, J. Wu, B. Zhou, Y. Hong, S. Lia and W. Wen, *Nanoscale*, 2013, **5**, 6167-6172
6 Y. Wei, S. Han, D. A. Walker, S. C. Warren and B. A. Grzybowski, *Chem. Sci*., 2012, **3**, 1090-1094
7 O. Akhavan, R. Azimirad, S. Safad and E. Hasanie, *J. Mater. Chem*., 2011, **21**, 9634-9640
8 S. A. Ansari, M. M. Khan, S. Kalathil, A. Nisar, J. Leea and M. H. Cho, *Nanoscale*, 2013, **5**, 9238-9246
9 S. Cho, J. Jang, J. S. Lee and K. Lee, *CrystEngComm*, 2010, **12**, 3929-3935
10 T. Liu, Q. Wang and P. Jiang, *RSC Adv*., 2013, **3**, 12662-12670
11 X. Wang, L. Yin, G.Liu, L. Wang, R. Saito, G. Q. Lu and H. Cheng, *Energy Environ. Sci*., 2011, **4**, 3976-3979
12 S. Ma, J. Xue, Y. Zhou and Z. Zhang, *J. Mater. Chem. A*, 2014, **2**, 7272-7280
13 S. Ma, J. Xue, Y. Zhou, Z. Zhang and X. Wu, *CrystEngComm*, 2014, **16**, 4478-4484
14 Y. Zhu, M. Li, Y. Liu, T. Ren, and Z. Yuan, *J. Phys. Chem. C* 2014, **118**, 10963-10971
15 Y. Lin, Y. Hsu, Y. Chen, L. Chen, S. Chend and K. Chen, *Nanoscale*, 2012, **4**, 6515-6519
16 Z. Wu, F. Dong, W. Zhao, H. Wang, Y. Liu and B. Guan, *Nanotechnology,* 2009, **20**, 235701
17 J. Xue, S. Ma, Y. Zhou and Z. Zhang, *New J. Chem.,* 2015, **39**, 1852-1857
18 L. Chena, Y. Tua, Y. Wanga, R. Kana, C. Huangb, *Journal of Photochemistry and Photobiology A: Chemistry.* 2008, **199**, 170-178
19 F. Dong, H. Wang, and Z. Wu, *J. Phys. Chem. C,* 2009, **113**, 38
20 Y. Lin, Y. Hsu, Y. Chen, L. Chen, S. Chend and K. Chen, *Nanoscale*, 2012, **4**, 6515-6519
21 Y. Zheng, X. Tao, Q. Hou, D. Wang, W. Zhou, and J. Chen, *Chem. Mater*., 2011, **23**, 1
22 C. Yin, S. Zhu, Z. Chen, W. Zhang, J. Gua and D. Zhang, *J. Mater. Chem. A*, 2013, **1**, 8367-8378
23 G. Liu, C. Han, M. Pelaez, D. Zhu, S. Liao, V. Likodimos, N. Ioannidis, A. G. Kontos, P. Falaras, P. S. M. Dunlop, J. A. Byrne and D. D. Dionysiou, *Nanotechnology*, 2012, **23**, 294003
24 P. Zhang, C. Shao, Z. Zhang, M. Zhang, J. Mu, Z. Guoab and Y. Liua, *Nanoscale*, 2011, **3**, 2943-2949
25 D.L. Liao, B.Q. Liao, *Journal of Photochemistry and Photobiology A: Chemistry,* 2007, **187**, 363-369
26 H. Lim, Y. Sun and K. Suh, *J. Mater. Chem. A*, 2013, **1**, 10107-10111
27 O. Haibo, H. J. Feng, L. Cuiyan, C. Liyun, F. Jie, *MaterialsLetters*,2013,**111**, 217-220
28 H. Kim, H. Lim, Y. Kim, Y. Sun and K. Suh, *RSC Adv*., 2014, **4**, 60573-60580
29 E. M. Maya, J. Benavente, J. Abajoa, *Materials Chemistry and Physics*,2012, **131**, 581- 588
30 K. Bang, H. Lim, S. Park and K. Suh, *RSC Adv*., 2015, **5**, 59257-9262

Graphical abstract

Carbon-doped ZnO Submicron Spheres Functionalized with Carboxylate Groups and Effect of Dispersion Stability in the Colloidal System for High Photocatalytic Activity

JaeSoul Lee‡[a], Hyung-Seok Lim‡[a] and Kyung-Do Suh*[a]

[a] *Department of Chemical Engineering, College of Engineering, Hanyang University, eoul, Republic of Korea, 133-791. E-mail: kdsuh@hanyang.ac.kr*

** Corresponding author (kdsuh@hanyang.ac.kr)*

‡ These authors contributed equally to this work.

This paper describes a new approach to improve the photodegradation efficiency using the carbon-doped ZnO submicron spheres in the colloidal system.